Cell Reports
Physical Science

Article

Dynamic interfacial vortex arrays for advanced antifouling

Graphical abstract

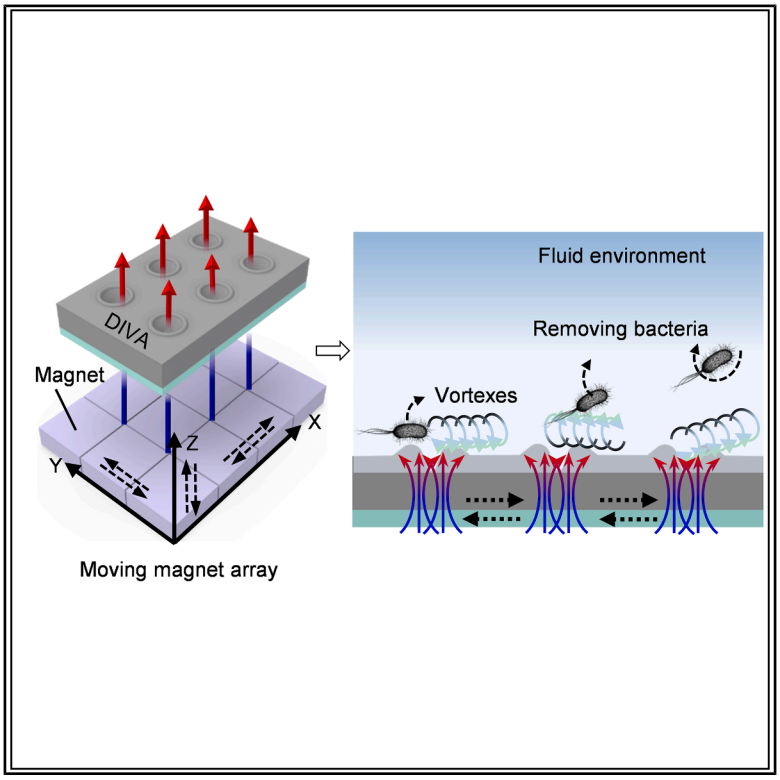

Authors

Zhongbao Wang, Yixing Chen, Decui Cheng, ..., Yuan Ma, Jing Wang, Li-Min Zhu

Correspondence

juw6@sjtu.edu.cn

In brief

Microbial fouling poses a persistent challenge for humans, ranging from infections from biomedical devices to malfunctions in industrial and maritime equipment. Wang et al. report a dynamic interfacial vortex array (DIVA) antifouling strategy that maintains surfaces with <2% fouling in high-concentration microbial solutions and achieves >95% microbe removal independent of microbial species.

Highlights

- A dynamic interfacial vortex array (DIVA) strategy for antifouling and fouling release
- DIVA keeps surfaces clean with <2% microbial attachment at high bacterial concentration
- DIVA removes >90% of biofilms and reduces to <10% fouling coverage within 1 h
- DIVA effectively avoids drug resistance and maintains prolonged antibacterial performance

Wang et al., 2025, Cell Reports Physical Science 6, 102727
August 20, 2025
https://doi.org/10.1016/j.xcrp.2025.102727

CellPress

Cell Reports
Physical Science

CellPress
OPEN ACCESS

Article

Dynamic interfacial vortex arrays for advanced antifouling

Zhongbao Wang,[1,2] Yixing Chen,[1] Decui Cheng,[3] Bin Wang,[5] Shuaidong Qi,[1] Yifan Xia,[5] Tingting Pan,[3] Hongping Qu,[3] Yuan Ma,[4] Jing Wang,[1,2,6,*] and Li-Min Zhu[1,2]

[1]School of Mechanical Engineering, Shanghai Jiao Tong University, Shanghai 200240, China
[2]State Key Laboratory of Mechanical System and Vibration, Shanghai Jiao Tong University, Shanghai 200240, China
[3]Department of Critical Care Medicine, Ruijin Hospital, Shanghai Jiao Tong University School of Medicine, 197 Ruijin Er Road, Shanghai 200025, China
[4]Department of Mechanical Engineering, Research Institute for Intelligent Wearable Systems, The Hong Kong Polytechnic University, Hong Kong 999077, China
[5]School of Aeronautics and Astronautics, Zhejiang University, Hangzhou 310027, China
[6]Lead contact
*Correspondence: juw6@sjtu.edu.cn
https://doi.org/10.1016/j.xcrp.2025.102727

SUMMARY

Microbial fouling is a persistent problem ranging from biomedical devices to industrial and maritime equipment. Current antifouling strategies fall short of durability due to the rapid degradation of the biocidal interfaces. Here, we report a dynamic interfacial vortex array (DIVA) antimicrobial strategy that can develop high wall shear forces to actively remove any adhered microbial species on the surface. The DIVA is induced by a reciprocating magnet array on a magnetic soft composite surface. The simulation results of the wall shear on the DIVA surface show that the average wall shear on the moving dimple is ~10 times that on the moving plate. This DIVA is able to keep a surface with <2% fouling in a high-concentration bacterial environment and demonstrates >90% bacterium removal within an hour independent of bacterial species. The proposed DIVA strategy effectively maintains prolonged antibacterial performance, showing profound potential in medical equipment, the food industry, and the maritime industry.

INTRODUCTION

Microbial fouling has posed significant hazards to human society in medical, maritime, and many other industries for thousands of years.[1–4] In medical settings, microbes may adhere to and grow on different surfaces, resulting in severe consequences, such as surgical infection, implant rejection, and malfunction of biosensors.[5,6] Marine microorganisms increase hull corrosion, drag, and fuel consumption by attaching to the ships' hulls, costing the maritime industry >$15 billion globally per year.[7] Industrial biofouling occurs in power plants, water-cooling systems, and the food industry, resulting in energy waste, pipeline blockage, and food insecurity.[8] Various microbial species use different nucleation, attachment, and biofilm formation mechanisms on different surfaces and evolve over time to survive man-made antibiotics. According to the prediction from the World Health Organization, drug-resistant bacterial infection will be the leading cause of death globally, resulting in $1 trillion of additional healthcare costs by 2050,[9] underscoring the urgency to develop biocompatible antimicrobial technologies that may decelerate the spread of surface microbial fouling.[10]

Current antimicrobial materials mainly adopt one of two passive strategies: (1) fouling release by low-adhesion surfaces[11,12] and (2) chemical or physical bactericidal methods.[13–15] The passive fouling release strategy adopts natural flow shear[16] or capillarity forces[17] at the liquid-air interface to effectively remove attached microbes or biofilms. This strategy relies heavily on the low interfacial work of adhesion by applying low-surface-energy chemicals,[18] superhydrophobicity,[11] or lubrication.[12] Such fouling release methods deteriorate quickly and easily by surface chemistry modification from various microbes, particularly in underwater environments. For example, superhydrophobic surfaces can maintain self-cleaning for years if droplets with microbes are only in short contact with them. However, they can only last for less than 1 day if submerged in microbial solutions.[19] Further complicating matters, it is highly challenging to restore the surface's superhydrophobicity once contaminated with microbes. Passive bactericidal methods, on the other hand, employ the gradual release of antibiotics, toxic chemicals,[14] or mechanical biocidal nanostructures.[20,21] The primary distinction between chemical and physical biocidal methods lies in their killing efficiency and mechanisms. Antimicrobial chemicals can destroy the cell membrane and remain antimicrobial until the exhaust of them. They only work for a range of microbes and will lead to drug resistance. The mechanical biocidal structures poke into the cell membrane, causing starvation and cell fluid leakage, and the killing of microbes only happens when they

are in contact with the nanostructures, resulting in a relatively low antimicrobial efficiency.[1]

Recent antimicrobial advances focus on active antimicrobial strategies with stimulus-responsive soft matter. These active strategies mostly remove attached microbes through dynamic surface deformation actuated by an electric[22] or magnetic field[23–25] that induces interface fracture or fluid shear. The interface fracture methodology needs a specific surface pattern for each microbial species and requires large energy storage in the materials to introduce the crack. Dynamically tuning the surface pattern using electrical stimulus-responsive materials is not only challenging but also potentially hazardous, since high voltages are usually unavoidable.[22] Fluid shear generated by magnetic responsive micro-cilia is achieved through careful mechanical design and complex manufacturing processes and is difficult to scale up and implement in a wide range of application scenarios.[24] More importantly, these active antimicrobial surfaces are more effective at removing biofilms than small clusters of microbes.[26] With their relatively high adhesion to various microbes, their ability to prevent early-stage microbial growth is usually limited.[27]

To overcome these challenges in antimicrobial methods, here, we propose an active and passive combined antimicrobial strategy based on dynamic interfacial vortex arrays (DIVAs) by magnetic-responsive dimples with ultra-low microbial adhesion. The magnetic-responsive DIVA material is composed of plasticized silicone uniformly infused with magnetic-responsive micro-neodymium-iron-boron (NdFeB) particles, which are magnetized after the crosslinking of the silicone polymer matrix, guaranteeing the NdFeB particles' magnetic orientation, and can promote >5 times greater surface deformation compared to other methods under the same magnetic field. DIVAs are generated by driving micro-dimple arrays using a reciprocatively moving magnet array and can develop higher wall shear forces from both normal and tangential direction compared to laminar shear flow. In addition, the velocity and vorticity of the DIVA can be controlled with different magnetic intensities and moving speeds. The visualized flow measurements demonstrate the fluid dynamics of the DIVA induced by a magnetic field. The ultra-low microbial adhesion is achieved by creating an organogel lubricated surface through swelling biocompatible low-surface-tension oil into the silicone polymer matrix. Compared with untreated silicone materials, the swollen plasticized silicone is able to reduce the adhesion toward various solid surfaces by up to 4 times, leading to fast removal of attached microbes. With such combined antimicrobial effects, the DIVA coating can keep surfaces <2% of microbial attachment in a high-concentration microbial solution and effectively remove attached microbes by >90% within an hour. With its readily attainable potential to scale up, we anticipate that this DIVA method can be implemented for diverse applications, including the maritime industry, biomedical implants, food processing, and more.

RESULTS

The fabrication and formation of the DIVA coating

The fabrication process of the DIVA coating is illustrated in Figure 1A. In particular, the coating solution, composed of a silicone base polymer, crosslinker, plasticizer (i.e., high-viscosity silicone oil), and NdFeB microparticles, was uniformly spin coated onto the substrate, followed by vacuum heating for curing. The high-viscosity silicone oil as a plasticizer works to soften the crosslinked polymer as well as enhance the suspension of NdFeB microparticles in the coating solution. Then, the crosslinked soft composite was directionally magnetized to saturation using a strong magnetic field of ~2 T. The DIVA coating was completed by swelling with low-viscosity silicone oil to create an ultra-low-adhesion surface.

As shown in Figure 1B, the commercially available permanent magnet units align as a square array, which is installed on a *z* axis lifting platform with in-plane motion ability. By precisely controlling the distance between the magnet array and the DIVA surface, the magnetic field intensity acting on the DIVA was quantitatively regulated. Under this magnetic actuation, concave dimple deformations on the DIVA surface were formed in similar arrays (Figure 1C). To note, these dimple arrays would move in plane, corresponding with the motion of the underlying magnet array (Figure 1D). As shown in a previous study,[17] the state-of-the-art surface with ultra-low-adhesion by interfacial lubrication is not able to prevent the settlement and growth of microbes, particularly in a static fluid environment (Figure 1E).

Specifically, we programmed the motion of the magnetic array in order to generate different dynamic dimple patterns, which would further generate interfacial vortices in a fluid environment (Figure 1F). The vorticity and velocity of vortices depend on the size and the moving speed of the dimples, which correspond to the magnetic field intensity and the mechanics of the DIVA materials. To this end, we systematically investigated the influence of the magnetic field intensity and characterized the mechanical and wetting property of the DIVA coating.

The properties of DIVA coatings with different compositions

Uniaxial tensile tests were conducted on the DIVA material to investigate the effects of the NdFeB content and the ratio of polydimethylsiloxane (PDMS) to silicone oil on their mechanical properties. As shown in Figure 2A, when the ratio of PDMS to silicone oil was 1:2, uniaxial tensile tests were conducted within a 0%–200% strain range on the DIVA coating with NdFeB contents of 20, 40, 60, and 80 wt %. The hysteresis of the stress-strain curve of the DIVA material gradually increased with the NdFeB content, demonstrating that the elastic modulus of the DIVA material increased with the increase in NdFeB content. Similarly, we fixed the NdFeB content as 40 wt % and applied the uniaxial tensile tests on the DIVA materials with different ratios of PDMS to silicone oil, from 2:1, to 1:1, to 1:1.5, and to 1:2. In this case, the hysteresis of the stress-strain curve of the DIVA material gradually decreased with the ratio of PDMS to silicone oil (Figure 2B). To balance the magnetic field-response deformation and the deformation recovery speed, 40 wt % NdFeB content and a 1:2 ratio of PDMS to silicone oil was determined as the DIVA material used in this work. The corresponding tensile strength is ~184.5 kPa, and the fracture strain can reach ~400% (Figure 2C).

To verify the low adhesion performance of the DIVA material, we measured the adhesion strength of the DIVA material

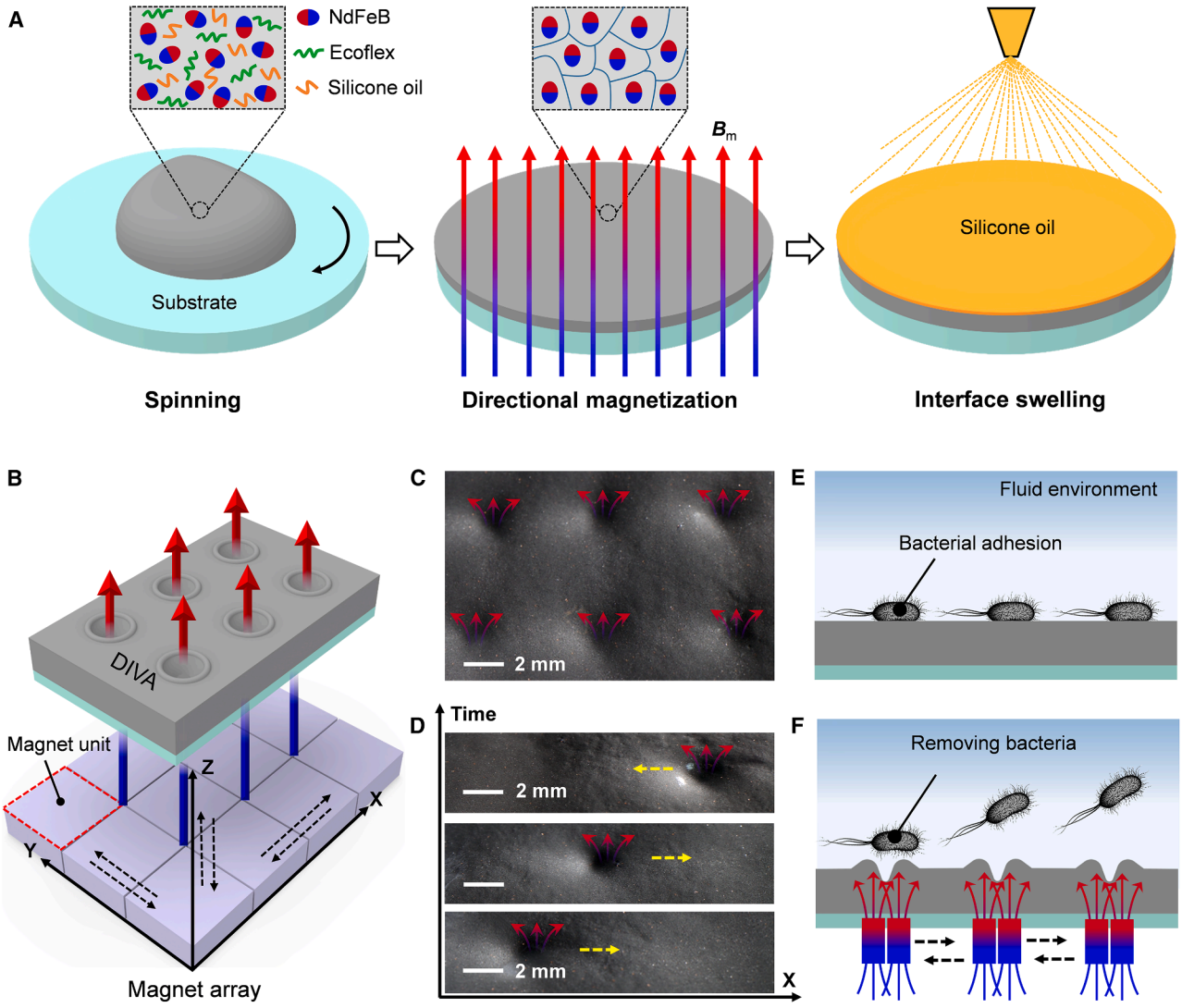

Figure 1. DIVA surface formation and antimicrobial strategy

(A) The fabrication process of the DIVA coating.

(B) Schematic of concave deformation of the DIVA coating driven by a magnet array.

(C) Optical image of concave deformation on the DIVA coating. Scale bar, 2 mm.

(D) The concave deformation on the DIVA coating moves with the movement of the magnet array along the *x* axis direction. Scale bar, 2 mm.

(E) Bacteria adhere to the static-state coating in a fluid environment.

(F) A reciprocating magnet array drives the DIVA coating to generate a dynamic concave deformation for inducing vortices to remove bacterial adhesion in a fluid environment.

toward different planar surfaces (Figure S1), including aluminum, soft PDMS (Ecoflex 00-30), and hard PDMS (Sylgard 184). These testing surfaces have a modulus spanning from 60 kPa to 11 MPa, simulating biological species from bacterial films to algae and barnacles. The adhesion strength of the DIVA material is ~100 Pa toward these materials, which is >5 times smaller compared to the unlubricated plasticized PDMS (Figure 2D).

As shown in Figure 2E, the water contact angle hysteresis of the DIVA coating was 4°, 5 times smaller than the non-swollen control surfaces. This indicates the slipperiness of the DIVA surface toward aqueous liquids. Interestingly, the plasticized PDMS with high viscosity silicone oil showed lower contact angle hysteresis compared to the one without plasticizer, implying that the surface of the plasticized PDMS contains free oil. In addition, the contact angle decreased from 97.4° to 76.8° after swelling with low-viscosity silicone oil (Figure 2F), which is caused by the wrapping meniscus of the oil. This effect also suggests that the swelling lubricant formed a lubricating layer that can replace the solid-solid interface into a liquid-liquid interface, therefore significantly reducing the interfacial work of adhesion.[28]

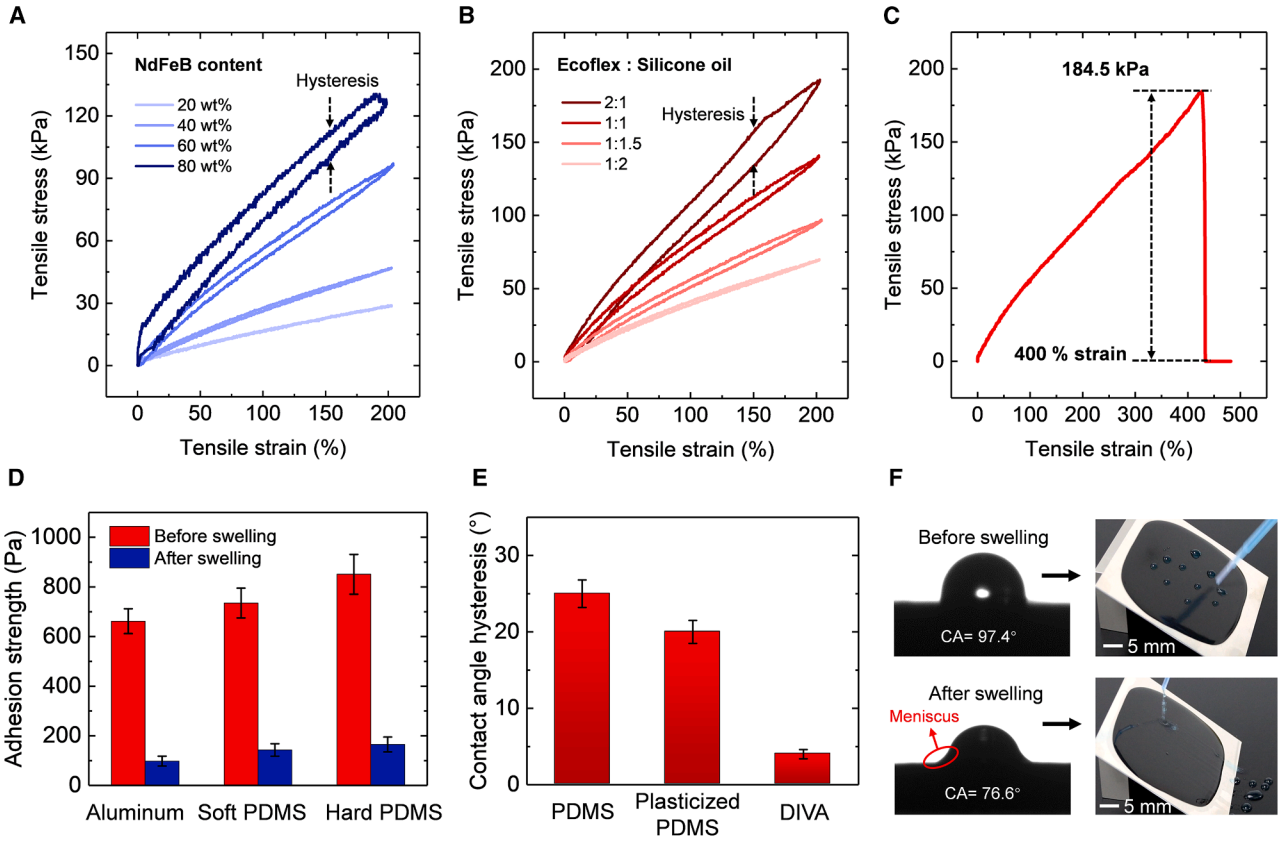

Figure 2. The mechanical properties and wettability of DIVA coatings with different compositions

(A) The stress-strain curves of the DIVA materials with NdFeB content of 20, 40, 60, and 80 wt %.

(B) The stress-strain curves of the DIVA materials with a ratio of Ecoflex to silicone oil of 2:1, 1:1, 1:1.5, and 1:2.

(C) The tensile strength of the DIVA with NdFeB content of 40 wt % and a ratio of Ecoflex to silicone oil of 1:2.

(D) The adhesion strength of the DIVA to aluminum, soft PDMS (Ecoflex 00-30), and hard PDMS before and after swelling with silicone oil.

(E) The contact angle hysteresis on the surface of PDMS, plasticized PDMS, and DIVA.

(F) Contact angle images and droplet sliding tests on the magnetic soft composites before and after swelling with silicone oil. Scale bar, 5 mm.

The error bars indicate the standard error obtained from 5 independent measurements.

The magnetic-responsive dimple deformation on the DIVA coating

We first embedded the commonly used magnetic Fe_3O_4 particles in the plasticized PDMS and measured the deformation response to the magnetic field. As the Fe_3O_4 particles are randomly distributed in the magnetic orientation (Figure S2A), the dimple deformation under a magnetic field of 300 mT had a depth of ~0.22 mm (Figures 3C, S2B, and S2C). In comparison, the magnetization was able to make the internal NdFeB particles holding a residual magnetism parallel to the magnetization direction (Figure 3A). With a magnetic particle content of 40 wt %, the DIVA coating with magnetized NdFeB particles can produce a concave dimple deformation with a diameter of 1.5 mm and a depth of >1 mm when applying a magnetic field of 300 mT (Figure 3B), at least 5 times larger than the deformation with Fe_3O_4 particles. By tuning the embedded magnetic particles, we can form dimple deformations on the DIVA with a scale spanning one order of magnitude, from 0.1 to 1 mm.

Furthermore, we explored the influence of the material composition and the magnetic field intensity on the dimple deformation of the DIVA coating. With a fixed magnetic field intensity (300 mT) and PDMS-to-silicone oil ratio (1:2), the dimple depth of the DIVA coating increases with the increase in NdFeB content (Figures 3D and S2D), from 0.25 mm with 20% particle content to ~0.8 mm with 40% particle content, and to ~1.1 mm with 60% particle content. The deformation depth increases more logarithmically with particle content percentage, indicating that the benefit of adding more particles for larger deformations decreases with higher particle content. In fact, the elastic modulus of the DIVA coating also increases with the increase in NdFeB content, which leads to a smaller deformation. In addition, it is more difficult to cure an NdFeB/PDMS composite with higher NdFeB content.

With a fixed NdFeB content (40 wt %), the dimple depth of the DIVA coating increases with the increase in the PDMS-to-silicone oil ratio (Figures 3E and S2E), from <0.2 mm with a 2:1 ratio to 0.4 mm with a 1:1.5 ratio and to ~0.8 mm with a 1:2 ratio. This corresponds with the elastic modulus of the DIVA material with different PDMS-to-silicone oil ratios, from ~40 kPa at the ratio of 1:2 to >100 kPa at the ratio of 2:1 (Figure 2B). It should be noted

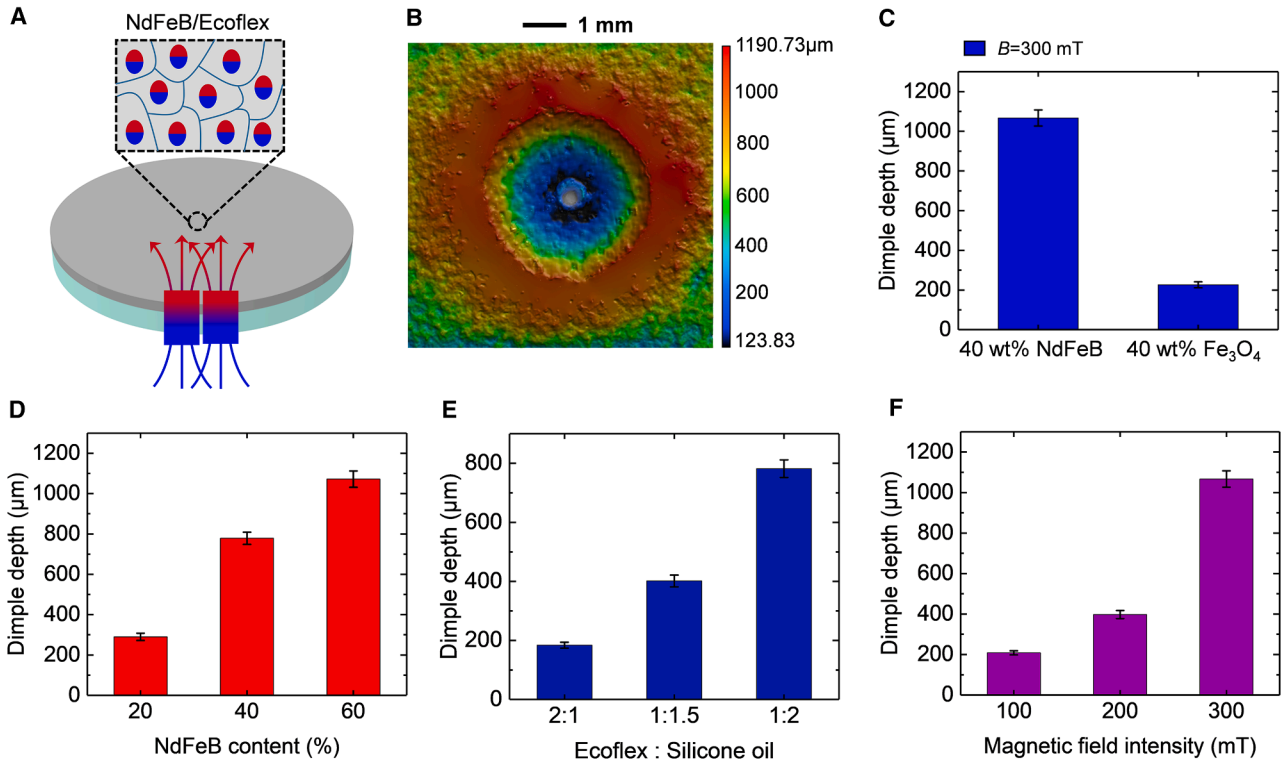

Figure 3. The magnetic-responsive dimple deformation on the DIVA coating

(A) Schematic of magnetic field-responsive concave deformation of the DIVA coating.

(B) Laser-scanning confocal microscopy image of the dimple deformation.

(C) The dimple depth of the NdFeB/Ecoflex composite and the Fe_3O_4/Ecoflex composite under the same conditions.

(D) The relationship between the dimple depth and NdFeB content.

(E) The relationship between the dimple depth and the ratio of Ecoflex to silicone oil.

(F) The relationship between the dimple depth and the magnetic field intensity.

The error bars indicate the standard error obtained from 5 independent measurements.

that, if the ratio of PDMS to silicone oil is small enough, then the DIVA material would be too soft to fully recover or have a short recovery response time after deformation. By changing the magnetic field intensity, as shown in Figures 3F and S2F, the dimple depth of the DIVA coating increases exponentially with the increase of the magnetic field intensity. In particular, a 300 mT magnetic field can generate a nearly 3 times larger surface deformation than 200 mT. Based on these experimental results, in order to achieve a large and quick deformation response on the DIVA, it is preferable to have magnetic particle content, a relatively soft polymer matrix, and a high driving magnetic field intensity. In addition, the thickness of the coating affects the dimple formation. As shown in Figure S3, when the coating thickness is less than 1.5 mm, the dimple depth increases approximately linearly with the coating thickness. When the coating thickness is greater than 1.5 mm, the dimple depth remains at ~1,050 μm. This indicates that the maximum deformation that magnetic soft materials can achieve under a 300-mT magnetic field is ~1,050 μm.

The visualized flow analysis of the DIVA coating

To investigate the interface fluid dynamics of a moving dimple deformation, we performed visualized flow measurements and numerical simulation of the wall shear on the DIVA surface. As shown in Figure S4, the visualized flow measurement setup consists of a solid-state laser, a high-speed camera, a rectangular transparent acrylic container with a DIVA sample at the bottom, and a magnet array installed on the stepper motor underneath (see methods). Different magnetic field intensities and moving speeds were applied to form a moving dimple on DIVA surfaces, generating interfacial vortexes that are captured and characterized by the visualized flow measurement setup (Figure 4A). The flow motion of the moving dimple is detailed in Figure 4B. Within the dimple structure, a circulating flow pattern is established, which not only exists within the concavity but also extends to the region above it. This circulating flow gives rise to the formation of a vortex.

In particular, before the passing-by of the magnet array, the DIVA coating is in a stationary state, and the interfacial fluids show a minimum-velocity field (Figure S5A; t = 5.97 s). When the magnet array moves along the x axis direction and passes by the visualized flow monitoring point, the interfacial fluid flows downward at an enhanced velocity (Figure S5A; t = 6.63 s). When the magnet array moves back at this monitoring point, the fluid experiences a reverse upward flow (Figure S5A; t = 7.46 s),

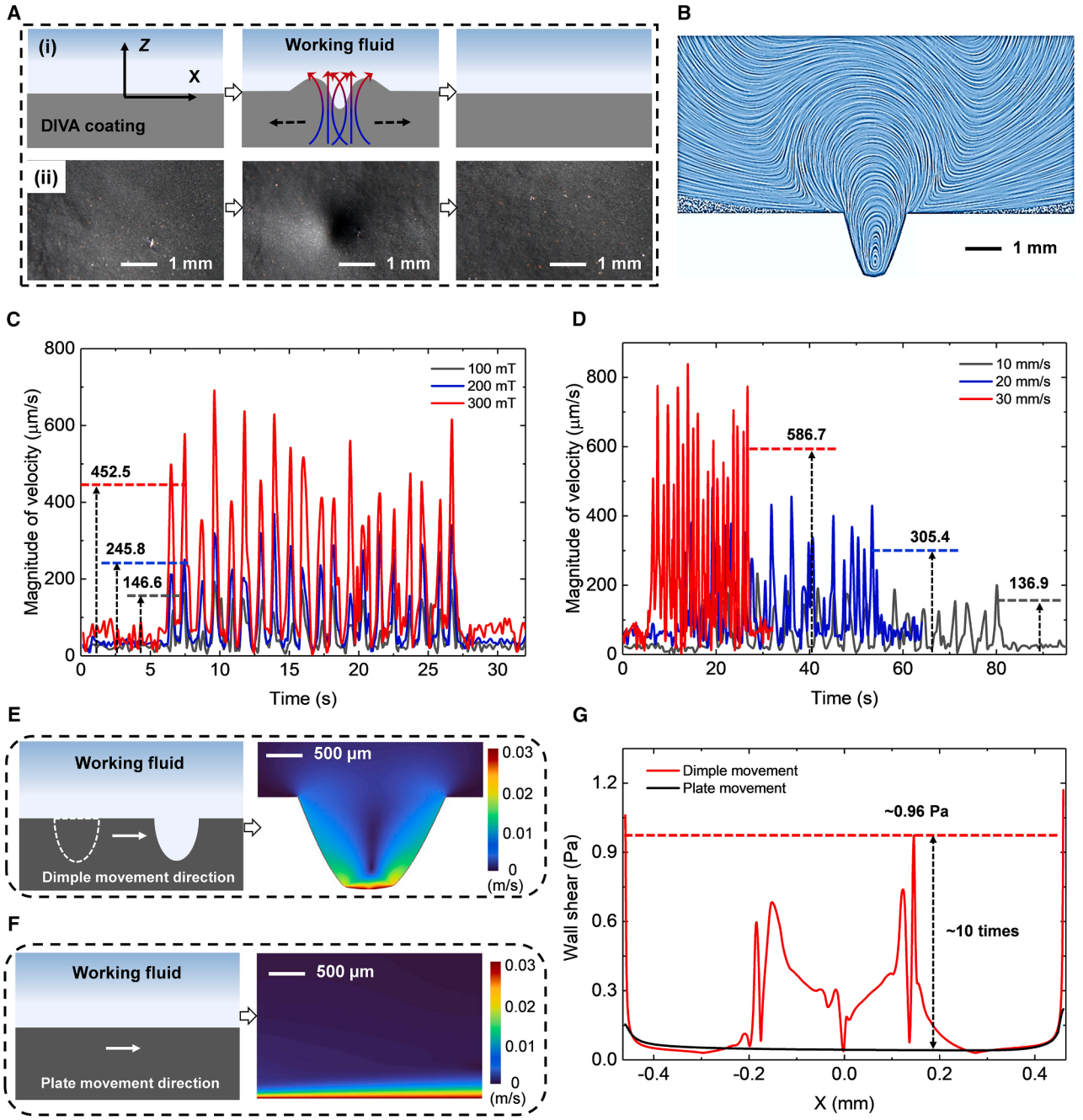

Figure 4. The analysis of the flow field on the DIVA surface

(A) Schematic of the visualized flow field measurement. Scale bar, 1 mm.

(B) The flow structure of the moving dimple.

(C) The flow velocity magnitude on the surface of the DIVA coating under driving magnetic fields of 100, 200, and 300 mT.

(D) The flow velocity magnitude on the surface of the DIVA coating under a motor motion speed of 10, 20, and 30 mm/s

(E) The velocity distribution of the moving dimple (30 mm/s).

(F) The velocity distribution of the moving plate (30 mm/s).

(G) Comparison of the wall shear for the moving dimple and moving plate.

as the moving direction is opposite. The corresponding flow velocity on the DIVA coating is presented in Figure S5B. The peak flow velocity in the *z* axis direction is ~600 μm/s, and the peak flow velocity in the *x* axis direction is ~450 μm/s. The flow velocity in the *x* axis and *z* axis directions exhibits periodic changes together with the cyclic motion of the magnet array

(Figure S5C). The visualized flow velocity field demonstrates the generation of vortices on the DIVA surface with a continuous propagation of dimple deformation. In addition, the propagation of reciprocating and repetitive dimple leads to the generation of global vortices along the *x* axis direction on the DIVA surface.

Further, we investigated the effects of the magnetic field density and the motion speed of the magnet array on the interfacial vortex. Specifically, the magnetic field intensity can be regulated by adjusting the distance between the magnet array and the DIVA coating, while the motion speed of the magnet array can be regulated by the stepper motor along the *x* axis direction. With a fixed speed of 30 mm/s, the average magnitude of the flow velocity (Figure 4C) on the DIVA surface is 146.6, 245.8, and 452.5 μm under magnetic fields of 100, 200, and 300 mT, respectively. This result demonstrates that the flow velocity increases with the magnetic field intensity under the same motion speed, as, correspondingly, the depth of the dimple increases with the magnetic field intensity as well (Figure 3F). With a fixed magnetic field intensity of 300 mT, the average magnitude of the flow velocity on the DIVA surface is 136.9, 305.4, and 586.7 μm under a motor motion speed of 10, 20, and 30 mm/s, respectively. The flow velocity increased by ∼4 times as the motor speed increased from 10 to 30 mm/s (Figure 4D). Therefore, in order to generate a stronger vortex for preventing microbial attachment on the DIVA, it is suggested that a larger dimple deformation and higher motion speed of the dimples are preferred. These application requirements also help to determine the parameter of DIVA material synthesis: soft polymer matrix (PDMS:silicone oil = 1:2), low mechanical hysteresis, and high magnetic response (magnetized NdFeB particle content: 40%).

To analyze the wall shear on the moving dimple, the numerical simulation of the wall shear on the DIVA surface was performed with the ANSYS Fluent software. We simulate the motion of the dimple and the plate separately (Figures 4E and 4F). The simulation results show that the average wall shear stress on the moving dimple is ∼10 times that on the moving plate (Figure 4G); this is because the vortex induced the moving dimple substantially increases the surface shear stress, further enhancing its antifouling ability. In contrast, the moving plate's lower and more uniform shear stress provides limited mechanical cleaning. Therefore, the moving dimple geometry is more effective in antifouling applications. A few studies[29–31] on this fluid shear effect found that the bacterial attachment decreased as shear stress increased. These studies also indicated that this shear effect is species and surface dependent. The critical shear can be in a wide range, from 10 to 1,000 mN/m^2. For example, the critical shear stress for *Escherichia coli*, *Staphylococcus aureus*, *Pseudomonas aeruginosa*, and *Staphylococcus epidermidis* was ∼850, 1,000, 1,100, and 2,700 mN/m^2, respectively, on a pristine silicone rubber surface.[32–35] In our study, bacterial adhesion on the DIVA surface decreases by ∼4.5 times compared to the silicone rubber (Figure 2D). This means the required shear stress on DIVA for *E. coli*, *S. aureus*, *P. aeruginosa*, and *S. epidermidis* is reduced to 190, 220, 240, and 600 mN/m^2, respectively. More importantly, the DIVA can develop a high wall shear stresses of ∼960 mN/m^2 (Figure 4G), which is higher than all of these required shear stresses to prevent bacterial fouling. Shear stress can effectively influence microbe settlement and corresponding biofilm formation,[36] as our experiment results and analysis indicate. There could be other factors that can also promote cell detachment and biofilm delamination, in particular in biological species; for example, dolphin skin dynamic wrinkles.[26]

The antifouling and fouling release testing of the DIVA coating

To test the antifouling performance of the DIVA coating, we select *E. coli* as the signature microbial. An *E. coli* cell suspension with a concentration of optical density 600 (OD_{600}) of 0.1 was cultured on a static surface and DIVA surfaces with different operational conditions for 12 h. The experimental platform of the *E. coli*-resistant assay of the DIVA coating is depicted in Figure S6. During the antifouling experiment, the reciprocating speed of the *y* axis stepper motor was set to 5 mm/s to ensure that the magnetic field-responsive dynamic deformation could fully cover the entire coating surface (see details in methods).

To obtain optimal antifouling operation parameters, we systematically investigated the effects of the driving magnetic field intensity (*B*: 100, 200, and 300 mT), motor motion speed (V_x: 10, 20, and 30 mm/s), and magnet unit area (*a*: 25, 100, and 225 mm^2) (Figure S7) on the antifouling performance of the DIVA surface. As shown in Figure 5A, the DIVA dynamic surfaces exhibited a greatly enhanced antifouling performance compared to that of the static surface. With fixed moving speed and magnet size (V_x = 30 mm/s and a = 25 mm^2), the areal coverage of bacteria on the DIVA surface decreased with the increase in magnetic field intensity *B* (Figure 5B). With fixed magnetic field intensity and magnet size (B = 300 mT and a = 25 mm^2), the areal coverage of bacteria on the DIVA surface decreased with the increase of the magnetic array moving speed V_x (Figure 5C). With fixed magnetic field intensity and moving speed (B = 300 mT and V_x = 30 mm/s), the areal coverage of bacteria on the DIVA surface decreased with the decrease in magnet size *a* (Figure 5D).

To further examine the antifouling performance of the DIVA coating, we also analyzed the effects of the antifouling operation parameters (B, V_x, and a) on the colony-forming units (CFUs) on the surface of the DIVA coating. Likewise, the CFUs on the static surface were much higher than on the DIVA surface (Figure S8), which further proves that the DIVA coating has better antifouling performance. With a fixed moving speed and magnet size (V_x = 30 mm/s and a = 25 mm^2), the CFUs on the surface of the DIVA coating decreased with the increase in *B* (Figure S9A). With fixed magnetic field intensity and magnet size (B = 300 mT and a = 25 mm^2), the CFUs on the surface of the DIVA coating decreased with the increase in V_x (Figure S9B). With fixed magnetic field intensity and moving speed (B = 300 mT and V_x = 30 mm/s), the CFUs on the surface of the DIVA coating increased with the increase in *a* (Figure S9C). These experimental results suggest an optimized external magnetic stimulation condition: (1) higher magnetic field intensity (B = 300 mT), (2) faster magnet array moving speed (V_x = 30 mm/s), and (3) smaller magnet size (a = 25 mm^2). With greater B and V_x, the velocity and vorticity of the induced vortices on the DIVA surface increase, which is more effective to prevent bacterial adhesion.

With the optimized stimulating magnetic field, we further explored the antifouling and the fouling-release performance of the DIVA surface with extensive fouling time. In particular, areal

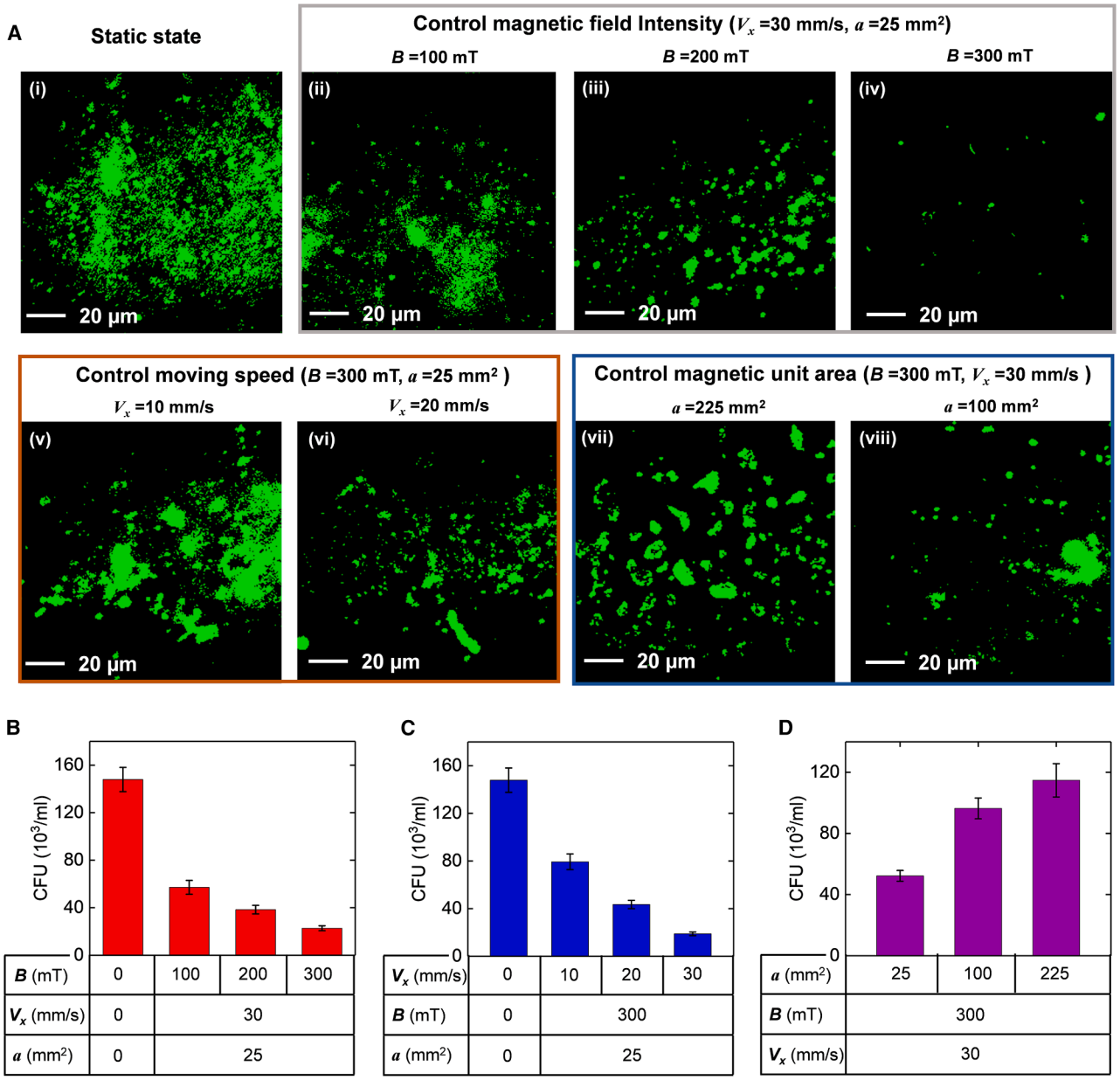

Figure 5. The effects of the operation parameters (*B*, V_x, and *a*) on the antifouling performance of the DIVA coating

(A) Confocal microscopy images of stained *E. coli* cells cultured (12 h at 37°C) on the static control surface and the DIVA coating surfaces with different operation parameters: (i) static control surface; (ii) B = 100 mT, V_x = 30 mm/s, and a = 25 mm^2; (iii) B = 200 mT, V_x = 30 mm/s, and a = 25 mm^2; (iv) B = 300 mT, V_x = 30 mm/s, and a = 25 mm^2; (v) B = 300 mT, V_x = 10 mm/s, and a = 25 mm^2; (vi) B = 300 mT, V_x = 20 mm/s, and a = 25 mm^2; (vii) B = 300 mT, V_x = 30 mm/s, and a = 225 mm^2; (viii) B = 300 mT, V_x = 30 mm/s, and a = 100 mm^2. Scale bars, 20 μm.

(B–D) The areal coverage percentage of the *E. coli* cells on the DIVA coating after antifouling testing with different operation parameters: (B) driving magnetic field intensity, (C) motor motion speed, and (D) magnet unit area. The error bars indicate the standard error obtained from 5 independent measurements.

coverage percentage and CFUs were used as the representative parameters to characterize the amount of the attached *E. coli*. Areal coverage percentage describes the total bacterial coverage in a two-dimensional manner; while CFUs characterize the total bacterial cells attached on the surface.

In the antifouling experiment, we simultaneously started the moving magnetic field when sterilized DIVA surfaces were placed in a high-concentration *E. coli.* solution, followed by incubation for 24 h. After 10 min, 1 h, and 24 h, we extracted the DIVA surface from the bacterial solution and measured the amount of bacteria on the surface. As shown in Figures 6A and S10A, the CFUs and areal coverage of *E. coli* cells on the DIVA coating after the antifouling test sharply decreased with time. When t > 1 h, the areal coverage of *E. coli* cells was <1% (Figure 6B), and the CFUs

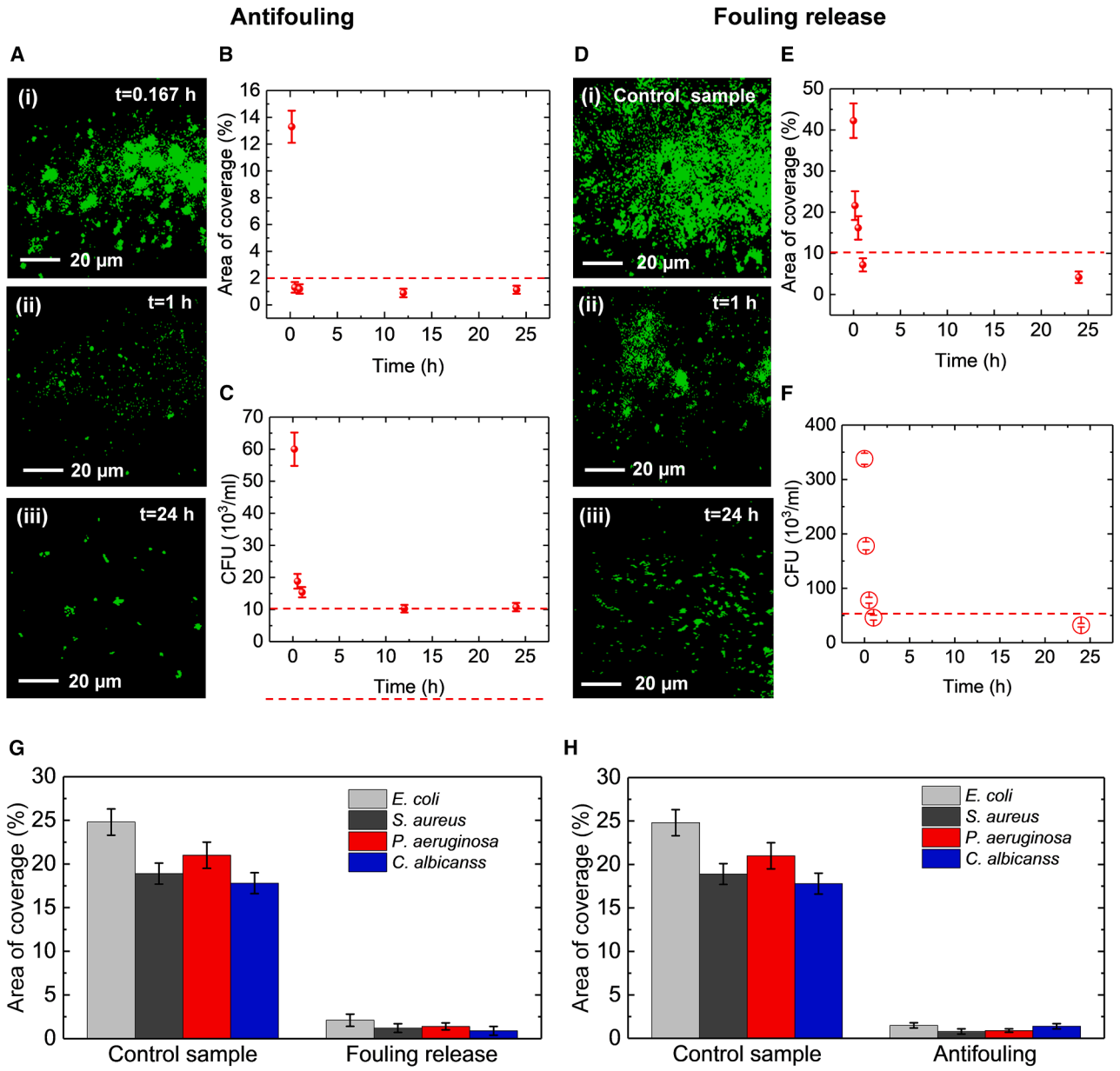

Figure 6. Antifouling and fouling release testing of the DIVA coating with optimal operation parameters (B = 300 mT, V_x = 30 mm/s, and a = 25 mm^2)

(A) Confocal microscopy images of the stained *E. coli* cells on the DIVA coating after antifouling tests with different magnetically actuated times: (i) t = 0.167 h, (ii) t = 1 h, and (iii) t = 24 h. Scale bars, 20 μm.

(B) The areal coverage of the *E. coli* cells on the DIVA coating after antifouling testing vs. the magnetically actuated time.

(C) The CFUs of the *E. coli* cells after antifouling testing vs. the magnetically actuated time.

(D) After *E. coli* cells were cultured on a static surface for 24 h at 37°C, confocal microscopy images of the stained *E. coli* cells on the DIVA coating were taken after fouling release tests with different magnetically actuated times: (i) control sample (t = 0 h), (ii) t = 1 h, and (iii) t = 24 h. Scale bars, 20 μm.

(E) The areal coverage of the stained *E. coli* cells on the DIVA coating after fouling release testing vs. the magnetically actuated time.

(F) The CFUs of the *E. coli* cells on the DIVA coating after fouling release testing vs. the magnetically actuated time.

(G and H) The areal coverage percentage of *E. coli*, *S. aureus*, *P. aeruginosa*, and *C. albicans* on the surface of the DIVA coating: (G) after antifouling testing for 24 h and (H) after fouling release testing for 24 h.

The error bars indicate the standard error obtained from 5 independent measurements.

on the DIVA coating remained at 10^4/mL (Figure 6C), with an antifouling efficiency exceeding 98%.

In the fouling release experiment, the DIVA coating samples were immersed in the *E. coli* cell suspension incubated at 37°C for 24 h for the biofilm formation.[37] Then, the DIVA surfaces were continuously magnetically actuated with optimal antifouling parameters (B = 300 mT, V_x = 30 mm/s, and a = 25 mm^2). Similarly, we found that the DIVA surface can efficiently keep the bacterial coverage area percentage at <10% within 1 h and effectively remove >90% of the biofilm within 24 h of actuation, as shown in Figures 6D–6F. The areal coverage of *E. coli* on the DIVA surface rapidly decreased in the first hour (Figure 6E). In addition, the CFUs of *E. coli* cells on the DIVA surface maintained at an extremely low level after the first hour (Figures 6F and S10B). For the antibacterial test, when the antifouling time (magnet movement time) is > 0.5 h, the antifouling efficiency exceeds 90%. The antifouling effect of the DIVA can almost instantly keep the surface free from bacteria settlement when the interfacial vortex continues moving at the optimized operation parameters. As shown in Figure S11, if the antifouling time is extended, then an antifouling efficiency of >99% can be achieved. When the antifouling time is greater than 48 h, the antifouling efficiency (*E. coli*) is greater than 99.5%. To make the experiment more convincing, the concentration of the bacterial solution sample we used during the experiment (OD_{600} of 0.1) was ~100 times higher than the clinical bacterial infection standard. When t > 36 h, the areal coverage of *E. coli* cells in the fouling release test was <1% (Figure 6B), and the CFUs on the DIVA coating remained at <10^4/mL in a high-concentration bacterial environment (Figure 6C), which is below the clinical standard for bacterial colonization.[38]

Different types of antibiofilm assays were performed, including *E. coli* (gram-negative bacterium), *S. aureus* (gram-positive bacterium), *P. aeruginosa* (drug-resistant bacterium), and *C. albicans* (fungus). The antifouling and fouling release testing of the DIVA coating was conducted with optimal operation parameters: B = 300 mT, V_x = 30 mm/s and a = 25 mm^2. Figure S12 demonstrates the antifouling and fouling release performance of the DIVA surface with *E. coli*, *S. aureus*, *P. aeruginosa*, and *C. albicans*. For the fouling release performance, after 24 h of DIVA stimulation, the areal coverage percentages of *E. coli* (Figures S12A(i), A(ii), and S12B), *S. aureus* (Figures S12C(i), C(ii), and S12D), *P. aeruginosa* (Figures S12E(i), E(ii), and S12F), and *C. albicans* (Figures S12G(i), G(ii), and S12H) dropped from 24.8%, 18.9%, 21.1%, and 17.8% to 1.5%, 1.2%, 1.5%, and 0.9%, respectively. The fouling release rate can reach 93%–95% for various microbes. For the antifouling performance, in a continuous DIVA stimulation for 24 h, the areal coverage percentages of *E. coli* (Figures S12A(iii) and S12B), *S. aureus* (Figures S12C(iii) and S12D), *P. aeruginosa* (Figures S12E(iii) and S12F), and *C. albicans* (Figures S12G(iii) and S12H) remained extremely low: 2.1%, 0.9%, 1.1%, and 1.6%, respectively. The antifouling efficiency can reach 98%, which is higher than most static antifouling strategies. Furthermore, the antifouling tests of ~72 h for *E. coli*., *S. aureus*, *P. aeruginosa*, and *C. albicans* are shown in Figure S13, which reveals that the long-term antifouling efficiency against *E. coli*, *S. aureus*, *P. aeruginosa*, and *C. albicans* exceeds 95%. More importantly, the magnetic driving time does not affect the growth of the *E. coli* cells with the same concentration, indicating that the DIVA coating does not alter the physiological characteristics (drug resistance) of the *E. coli* cells (Figure S14).

Therefore, the designed DIVA coating can effectively prevent various types of bacteria, including *E. coli*., *S. aureus*, *P. aeruginosa*, and *C. albicans*, with both antifouling and fouling-release efficiency of 95%–99% (Figures 6G and 6H). We can anticipate that the DIVA technology has broad potential for applications associated with microbial fouling.

We further tested the environmental stability of the DIVA by soaking it in hydrochloride acid for a week and by heating it at 150°C for 3 days. The acid soaking had no impact on the antifouling property of the DIVA coating, as it remained at 98% antifouling efficiency after a week in acid (Figure S15A). In addition, the DIVA coating still demonstrated an antifouling efficiency of >95% after heating at 150°C for 3 days (Figure S15B). We also applied mechanical abrasion to the DIVA coating (see details in methods). As shown in Figure S16A, there were some scratches on the coating surface after the abrasion (Figure S16A(ii)). When re-swelling with silicone oil, the abraded DIVA surface reverted to the same smooth surface (Figure S16A(iii)). After fouling release and antifouling tests, the areal coverage percentage decreased from ~36% to ~3.8% and 3.6%, respectively (Figure S16B). The antifouling efficiency of the DIVA coating after abrasion exceeds 85%, while the interface re-swelling can restore its antifouling and fouling release efficiency back to >98% (Figure S16C). In addition, we extended the microbe fouling time to 7 days for *E. coli* and *S. aureus*. The areal coverage percentage of *E. coli* and *S. aureus* (Figure S17) was 1.5% and 1.9% on the DIVA compared to control surfaces at 50.5% and 46.8%, respectively. The long-term (7-day) antifouling efficiency against infectious microbes exceeds 95%.

Furthermore, we used a marine alga, *Platymonas subcordiformis*, as the biofoulant to test the antifouling performance of the DIVA in a marine environment. In particular, the coverage area percentage of marine algae on the control sample and DIVA after 7 days of submerging in the fouling solution is 52.8% and 1.2%, respectively (Figure S18). The control surface was a flat PDMS. The antifouling efficiency of DIVA toward marine algae can reach >97%, which is higher than many static anti-marine fouling methods.[7,39] This result indicates the potential of the DIVA technology to be implemented in the maritime industry.

More importantly, the long-term movement of the magnetic field does not cause a temperature change (Figure S19). Because the magnetic soft material based on NdFeB has a narrow hysteresis loop and minimal hysteresis loss (Figures 2A and 2B). The antifouling durability of our DIVA technology depends on the residual magnetism of the internal magnetic particles after magnetization. Therefore, as long as the external driving magnetic field strength (<300 mT) is less than the coercive force of the magnetic particles (NdFeB > 600 mT), the magnetic driving deformation of the DIVA coating remains basically unchanged. In addition, the low adhesion property of the DIVA can also be reserved for years based on previous studies.[40–42]

DISCUSSION

In summary, we developed a DIVA strategy to effectively and efficiently achieve both antifouling and fouling release by a

magnetic-responsive soft elastomer with interfacial lubrication. The optimized DIVA surfaces can rapidly respond to a magnetic field and dynamically generate high-aspect-ratio dimples, which produce vortices and shear flow to prevent any microbial attachment. The experimental results demonstrated that NdFeB particles in the elastomer with directional saturation magnetization can achieve larger magnetic field-responsive deformation than Fe_3O_4 or other magnetic particles. Through thorough mechanical analysis of DIVA materials with different compositions, an optimum DIVA with an NdFeB content of 40 wt % and a PDMS-to-silicone oil ratio of 1:2 was determined. With further interfacial lubrication, the adhesion strength of the DIVA to various solid surfaces was reduced by >5 times. The numerical simulation results of the wall shear on the DIVA surface show that the average wall shear on the moving dimple was ~10 times that on the moving plate, which confirms that the moving dimple geometry is more effective in antifouling applications. The visualized flow measurements and the antifouling experiments simultaneously optimized the condition for an effective DIVA antimicrobial strategy. The numerical simulation results of the wall shear on the DIVA surface show that the average wall shear on the moving dimple was ~10 times that on the moving plate. The DIVA strategy is capable of keeping surfaces clean with <2% microbial attachment in a high-concentration bacterial incubation environment for a long period of time. Further, it can remove 90% of biofilms and keep surfaces with <10% fouling in 1 h. Such simultaneous antifouling and fouling release performance cannot be achieved by state-of-the-art passive antimicrobial surfaces. More importantly, this strategy requires minimal energy input and does not cause any drug resistance.

The DIVA material is a super-elastomer composed of magnetic nanoparticles and silicone with the largest deformation of ~50% of compression under a magnetic field of 300 mT. As long as the external driving magnetic field intensity (<300 mT) is less than the coercive force of the magnetic particles (NdFeB > 600 mT), the magnetic field-responsive deformation of the DIVA coating remains unchanged. Therefore, the DIVA coating is estimated to have a highly sustained antifouling activity. Although this work only focuses on using magnetic fields to control the surface deformations of coatings, other actuation methods (ultrasound, electric field, light field, and thermal field) can also be used to achieve surface deformation of coatings, enabling a broader range of applications in the future. In addition, the DIVA strategy is estimated to cost only \$0.05/m^2/day for a continuous antifouling performance, which is 18 times cheaper than using current alcohol sterilization (see the detailed cost analysis in Note S1 and Table S1). Such a comparison is particularly valuable for the aquaculture industry, which usually uses UV or antibiotics for treating salmonid pathogens.[43]

In particular, zwitterionic polymer surfaces can form a stable hydration layer.[44,45] This ordered water layer is highly effective to prevent protein adhesion, which has been used by microbes to adhere on surfaces and to form biofilms. Magnetic micro-robots are stimulated to fracture biofilms and achieve a fouling release performance of ~70%,[25,46] but they cannot prevent biofouling. The mechanical biocidal effect from high-aspect-ratio nanostructures takes inspiration from dragonfly wing surfaces and is able to achieve antifouling up to 80% in a harsh fouling environment.[15,20,21] Slippery liquid-infused porous surfaces (SLIPSs) can release bacterial fouling by its extreme low surface adhesion. As the bacterial solution is not static, SLIPSs can even achieve almost no fouling.[12,28,40] Dynamic surface deformation has also been proposed to prevent biofouling. Such deformation can be stimulated from an electric[22] or magnetic[24] field. Although this method can reach ~90% antifouling, it cannot effectively prevent biofouling.

More importantly, the DIVA method is 4 orders of magnitude more durable than using alcohol sterilization[47] or mechanical biocide nanostructures[15,20,21] and 2 to 5 times more durable than state-of-the-art methods, including zwitterions,[44,45] SLIPSs,[12,28,40] UV sterilization,[48] magnetic robots,[25,46] and dynamic surface deformation[22,24] (Figure 7B). Therefore, we anticipate that the DIVA antimicrobial strategy can start a new sustainable chapter for preventing microbial fouling in a wide range of industrial, medical, and household settings.

METHODS

Materials

Ecoflex 00-30 was purchased from Smooth-on (USA). NdFeB microparticles with average sizes of 1–5 μm were purchased from Shanghai New Materials (China). SYLGARD 184 and silicone oil with a viscosity of 100–5,000 cSt was purchased from Dow Corning (USA).

Preparation of the DIVA coating

10 g Ecoflex 00-30 part A, 10 g Ecoflex 00-30 part B, and 40 g silicone oil with a viscosity of 1,000 cSt were sequentially added to a 100 mL beaker and fully mixed and debubbled by using a planetary centrifugal mixer (AR-100 THINKY; mixing protocol, 1 min; defoaming, 1 min). Then, 40 g NdFeB microparticles were added to the Ecoflex/silicone oil mixture, followed by stirring at 1,000 rpm for 5 min and vacuum defoaming. Next, the DIVA solution was uniformly spin coated onto a substrate at a speed of 100 rpm to prepare the DIVA coating with thickness of 5 mm and left to stand at room temperature for 5 min. The substrate can be metal, ceramic, glass, wood, or plastic. After spin coating, the DIVA sample was transferred to a vacuum oven and cured at 80°C for 2 h under a vacuum. After the magnetic soft composite solution was completely cured, a magnetic field of ~2 T was applied to magnetize the embedded NdFeB microparticles to saturation, followed by spraying a thin layer of silicone oil with a viscosity of 10 cSt for interface swelling for ~2 h to complete DIVA coating.

Adhesion measurement

The effective contact area in this test is 0.01 mm^2 with a loading force of 10 N. After 30 s of relaxation, the testing surface is pulled away from the planar surfaces with a speed of 10 mm/min. During this pulling process, normal forces are recorded with time, and the maximum force is regarded as the adhesion force. The

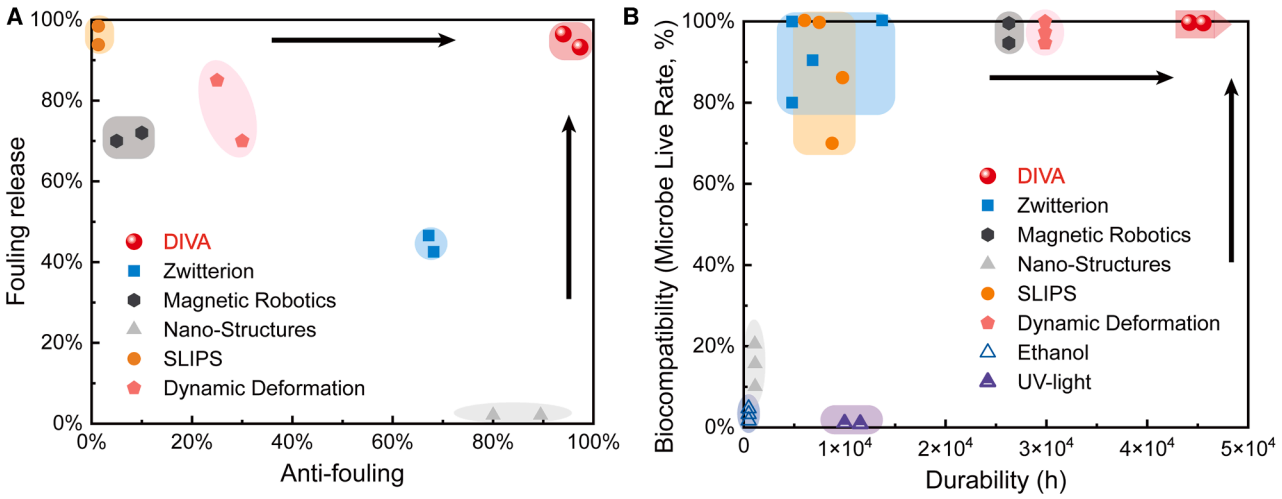

Figure 7. Comparison of different antifouling and fouling release strategies for performance, durability, and biocompatibility

(A) Anti-fouling and fouling release performance of different strategies, including zwitterion,[44,45] magnetic robotics,[25,46] nanostructures,[15,20,21] slippery liquid-infused porous surfaces (SLIPSs),[12,28,40] dynamic deformation,[22,24] and our DIVA technology.

(B) Durability and biocompatibility among different antifouling strategies, including zwitterion,[44,45] magnetic robotics,[25,46] nanostructures,[15,20,21] SLIPSs,[12,28,40] dynamic deformation,[22,24] ethanol sterilization,[47] UV light treatment,[48] and our DIVA technology. The biocompatibility is quantified by the microbe live rate when in contact with the surface or the materials used for antifouling.

adhesion strength is calculated as adhesion force divided by the contacting area.

Visualized flow measurement

The visualized flow measurement experimental setup consists of a solid-state laser, a high-speed camera, a rectangular transparent container with DIVA coating at the bottom, and a magnet array installed on a stepper motor. Polymethyl methacrylate (PMMA) particles with an average diameter of 20–50 μm were used as tracers. NaCl solution with a mass concentration of 0.5 g/mL with 0.5 mg/mL PMMA particles was added to the container. A high-speed camera with an effective pixel size of 10 μm was used to capture continuous images of the fluid at a frame rate of 100 fps and an exposure time of 1/300 s. The PIVlab plugin in MATLAB was used to process the particle images trace captured by the high-speed camera, thereby obtaining instantaneous velocity field information for analyzing the fluid flow near the deformation area. Four magnets form a rectangular shape, and the center of them generates a single dimple on the DIVA surface. The magnetic field intensity is 300 mT. A linear cyclic motion is applied to this dimple with a constant speed of 30 mm/s and a moving distance of 60 mm.

Numerical simulation of the wall shear

To analyze the wall shear on one moving dimple, the commercial CFD software ANSYS Fluent is used based on the Reynolds-averaged Navier-Stokes method. The moving velocity of the dimple and the control plate is set as 30 mm/s. Based on the moving velocity and diameter of the dimple, the Reynolds number is set to ~50. When the water flows through the dimple, even if the overall Reynolds number is low, local turbulence may be triggered by the moving boundary. We adopt the condition of a moving boundary, so the k - ε turbulence model is generally adopted in the present work.

Antibacterial assay

E. coli cells were cultured in 5 mL lysogeny broth (LB) medium (LB broth Miller) using an incubator shaker (Blue Pard, China) at 200 rpm and 37°C for 12 h, and then the bacterial concentration was measured using a P4 UV-visible spectrophotometer (MAPADA, China) at a wavelength of 600 nm (OD_{600}) to obtain an OD_{600} of 0.3. Next, the suspended culture medium was separated by a centrifuge (Beckman Coulter Genomics, USA) at a speed of 4,000 rpm for 5 min and replaced with a new culture medium. The bacteria were cultured at 37° C for 2 h, and then the concentration was adjusted to OD_{600} of 0.1.

For antifouling testing, the DIVA coating samples were sprayed with alcohol (70 vol %), followed by irradiation with a UV lamp (50 W, 365 nm) for 2 min. Then, the DIVA coating samples were immersed in a bacterial suspension for different times at 37°C. During this process, the DIVA coating samples were continuously magnetically actuated with a different magnetic field intensity (B), motor motion speed (V_x), and magnet unit area (a). We can obtain optimal antifouling operation parameters through extensive experiments. For fouling release testing, the DIVA coating samples were immersed in the bacterial suspension, followed by incubation for 24 h at 37°C. After incubation for 24 h, the DIVA coating samples were continuously magnetically actuated with optimal antifouling operation parameters.

To quantify the areal coverage, the DIVA coating samples were prepared in multiple groups and incubated simultaneously under the same conditions. After antifouling and fouling release tests with different operation parameters (B, V_x, and a) were completed, the DIVA coating samples were

rinsed three times with phosphate-buffered saline (PBS), and then the DIVA coating samples were stained using a fluorescent labeling reagent (excitation wavelength, 488 nm). The stained samples were kept in a dark environment at room temperature for 30 min and rinsed twice with PBS solution. Next, the samples were monitored with a high-resolution laser confocal microscope (Leica, STELLARIS 5). Subsequently, the areal coverage of the stained bacteria was analyzed using ImageJ software.

For the CFU assay, after completing antifouling and fouling release testing with different operation parameters, the DIVA coating samples were rinsed three times with PBS solution, transferred into a beaker containing 10 mL sterile PBS, and sonicated in a water bath for 2 min at 350 Hz to remove all bacteria from the surface of the DIVA coating samples. The serially diluted bacterial solution was plated on an LB agar surface and incubated for 24 h at 37°C. Finally, the grown bacteria were counted to quantify the CFUs.

Algae fouling experiment

15 mL of seawater and culture medium were added to two Petri dishes containing DIVA coating samples. Then, 5 mL of *P. subcordiformis* was added to each dish. We gently mixed the algae, avoiding vigorous shaking that could lead to cell damage and death. The experimental group of DIVA coating samples was continuously magnetically actuated with optimal antifouling operational parameters, while the control group was maintained without magnetic actuation under the same environmental conditions. The samples were cultured at room temperature with a 12-h light cycle for 7 days. After 7 days, the seawater containing the algae was removed, and the surfaces of the DIVA coating samples were gently rinsed three times with seawater. Subsequently, the samples were monitored with an optical microscope, and the algal coverage area was analyzed using ImageJ software.

Abrasion test

The Taber abrasion test was performed using a 5750 linear abrader from Taber Industries. We used the maximum abrasion speed of 60 cycles/min with a 50 mm travel distance per cycle, a harsh abrader (CS-10), and high loading weight (350 g). The abrader was roughened before all abrasion tests, following the instructions from Taber Industries. Each Taber abrasion test used a newly prepared abrader.

RESOURCE AVAILABILITY

Lead contact

Requests for further information, resources, and reagents should be directed to and will be fulfilled by the lead contact, Jing Wang (juw6@sjtu.edu.cn).

Materials availability

This study did not generate new unique reagents.

Data and code availability

- This study did not generate/analyze datasets/code.
- This study did not generate/analyze datasets/code.
- Any additional information required to reanalyze the data reported in this paper is available from the lead contact upon request.

ACKNOWLEDGMENTS

This work is supported by the National Natural Science Foundation of China (BE0200017 and BC0201038), the Shenlan Program from Shanghai Jiao Tong University (SL2022MS004), and the State Key Laboratory of Mechanical Systems and Vibration (MSVZD202401). Z.W. is grateful for funding support from the Postdoctoral Fellowship Program of CPSF (GZC20231584) and the China Postdoctoral Science Foundation (2024M761956).

AUTHOR CONTRIBUTIONS

J.W. and H.Q. conceived and designed the project. Z.W., T.P., D.C., S.Q., and Y.C. performed the experiments, including materials preparation, structural characterization, and device measurements. B.W. and Y.X. performed the simulation calculations. Z.W., J.W., and Y.M. wrote the manuscript. J.W. and L.-M.Z. supervised the project. All authors discussed and commented on the manuscript.

DECLARATION OF INTERESTS

The authors declare no competing interests.

SUPPLEMENTAL INFORMATION

Supplemental information can be found online at https://doi.org/10.1016/j.xcrp.2025.102727.

Received: December 27, 2024
Revised: April 16, 2025
Accepted: June 27, 2025
Published: July 25, 2025

REFERENCES

1. Linklater, D.P., Baulin, V.A., Juodkazis, S., Crawford, R.J., Stoodley, P., and Ivanova, E.P. (2021). Mechano-bactericidal actions of nanostructured surfaces. Nat. Rev. Microbiol. *19*, 8–22. https://doi.org/10.1038/s41579-020-0414-z.
2. Dhyani, A., Wang, J., Halvey, A.K., Macdonald, B., Mehta, G., and Tuteja, A. (2021). Design and applications of surfaces that control the accretion of matter. Science *373*, eaba5010. https://doi.org/10.1126/science.aba5010.
3. Munk, P., Brinch, C., Møller, F.D., Petersen, T.N., Hendriksen, R.S., Seyfarth, A.M., Kjeldgaard, J.S., Svendsen, C.A., van Bunnik, B., Berglund, F., et al. (2022). Genomic analysis of sewage from 101 countries reveals global landscape of antimicrobial resistance. Nat. Commun. *13*, 7251. https://doi.org/10.1038/s41467-022-34312-7.
4. Wan, F., Torres, M.D.T., Peng, J., and de la Fuente-Nunez, C. (2024). Deep-learning-enabled antibiotic discovery through molecular de-extinction. Nat. Biomed. Eng. *8*, 854–871. https://doi.org/10.1038/s41551-024-01201-x.
5. Dubern, J.F., Hook, A.L., Carabelli, A.M., Chang, C.Y., Lewis-Lloyd, C.A., Luckett, J.C., Burroughs, L., Dundas, A.A., Humes, D.J., Irvine, D.J., et al. (2023). Discovery of a polymer resistant to bacterial biofilm, swarming, and encrustation. Sci. Adv. *9*, eadd7474. https://doi.org/10.1126/sciadv.add7474.
6. Leslie, D.C., Waterhouse, A., Berthet, J.B., Valentin, T.M., Watters, A.L., Jain, A., Kim, P., Hatton, B.D., Nedder, A., Donovan, K., et al. (2014). A bioinspired omniphobic surface coating on medical devices prevents thrombosis and biofouling. Nat. Biotechnol. *32*, 1134–1140. https://doi.org/10.1038/nbt.3020.
7. Callow, J.A., and Callow, M.E. (2011). Trends in the development of environmentally friendly fouling-resistant marine coatings. Nat. Commun. *2*, 244. https://doi.org/10.1038/ncomms1251.
8. Fan, S., Zhou, Q., Liu, C., Li, C., Ye, P., Tao, Y., Shao, H., Long, M., Zhang, Q., Li, Q., and Guo, X. (2024). Rational design of dynamic fibre membrane

for sustainable biofouling control. Nat. Water *2*, 161–171. https://doi.org/10.1038/s44221-024-00196-8.

9. Murray, C.J.L., Ikuta, K.S., Sharara, F., Swetschinski, L., Robles Aguilar, G., Gray, A., Han, C., Bisignano, C., Rao, P., Wool, E., et al. (2022). Global burden of bacterial antimicrobial resistance in 2019: a systematic analysis. Lancet *399*, 629–655. https://doi.org/10.1016/S0140-6736(21)02724-0.
10. Naghavi, M., Vollset, S.E., Ikuta, K.S., Swetschinski, L.R., Gray, A.P., Wool, E.E., Robles Aguilar, G., Mestrovic, T., Smith, G., Han, C., et al. (2024). Global burden of bacterial antimicrobial resistance 1990-2021: a systematic analysis with forecasts to 2050. Lancet *404*, 1199–1226. https://doi.org/10.1016/S0140-6736(24)01867-1.
11. Zhan, Y., Yu, S., Amirfazli, A., Rahim Siddiqui, A., and Li, W. (2022). Recent Advances in Antibacterial Superhydrophobic Coatings. Adv. Eng. Mater. *24*, 2101053. https://doi.org/10.1002/adem.202101053.
12. Wong, T.-S., Kang, S.H., Tang, S.K.Y., Smythe, E.J., Hatton, B.D., Grinthal, A., and Aizenberg, J. (2011). Bioinspired self-repairing slippery surfaces with pressure-stable omniphobicity. Nature *477*, 443–447. https://doi.org/10.1038/nature10447.
13. Kohanski, M.A., Dwyer, D.J., and Collins, J.J. (2010). How antibiotics kill bacteria: from targets to networks. Nat. Rev. Microbiol. *8*, 423–435. https://doi.org/10.1038/nrmicro2333.
14. Dhyani, A., Repetto, T., Bartikofsky, D., Mirabelli, C., Gao, Z., Snyder, S.A., Snyder, C., Mehta, G., Wobus, C.E., VanEpps, J.S., and Tuteja, A. (2022). Surfaces with instant and persistent antimicrobial efficacy against bacteria and SARS-CoV-2. Matter *5*, 4076–4091. https://doi.org/10.1016/j.matt.2022.08.018.
15. Jenkins, J., Mantell, J., Neal, C., Gholinia, A., Verkade, P., Nobbs, A.H., and Su, B. (2020). Antibacterial effects of nanopillar surfaces are mediated by cell impedance, penetration and induction of oxidative stress. Nat. Commun. *11*, 1626. https://doi.org/10.1038/s41467-020-15471-x.
16. Banerjee, I., Pangule, R.C., and Kane, R.S. (2011). Antifouling Coatings: Recent Developments in the Design of Surfaces That Prevent Fouling by Proteins, Bacteria, and Marine Organisms. Adv. Mater. *23*, 690–718. https://doi.org/10.1002/adma.201001215.
17. Tesler, A.B., Kim, P., Kolle, S., Howell, C., Ahanotu, O., and Aizenberg, J. (2015). Extremely durable biofouling-resistant metallic surfaces based on electrodeposited nanoporous tungstite films on steel. Nat. Commun. *6*, 8649. https://doi.org/10.1038/ncomms9649.
18. Callow, M.E., and Fletcher, R.L. (1994). The influence of low surface energy materials on bioadhesion — a review. Int. Biodeterior. Biodegrad. *34*, 333–348. https://doi.org/10.1016/0964-8305(94)90092-2.
19. Hwang, G.B., Page, K., Patir, A., Nair, S.P., Allan, E., and Parkin, I.P. (2018). The Anti-Biofouling Properties of Superhydrophobic Surfaces are Short-Lived. ACS Nano *12*, 6050–6058. https://doi.org/10.1021/acsnano.8b02293.
20. Ivanova, E.P., Hasan, J., Webb, H.K., Gervinskas, G., Juodkazis, S., Truong, V.K., Wu, A.H.F., Lamb, R.N., Baulin, V.A., Watson, G.S., et al. (2013). Bactericidal activity of black silicon. Nat. Commun. *4*, 2838. https://doi.org/10.1038/ncomms3838.
21. Wang, J., Macdonald, B., Cho, T.H., Repetto, T., Sun, K., Tuteja, A., and Dasgupta, N.P. (2024). Bioinspired Zwitterionic Nanowires with Simultaneous Biofouling Reduction and Release. Small *20*, 2400784. https://doi.org/10.1002/smll.202400784.
22. Shivapooja, P., Wang, Q., Orihuela, B., Rittschof, D., López, G.P., and Zhao, X. (2013). Bioinspired Surfaces with Dynamic Topography for Active Control of Biofouling. Adv. Mater. *25*, 1430–1434. https://doi.org/10.1002/adma.201203374.
23. Ko, H., Park, H.-H., Byeon, H., Kang, M., Ryu, J., Sung, H.J., Lee, S.J., and Jeong, H.E. (2019). Undulatory topographical waves for flow-induced foulant sweeping. Sci. Adv. *5*, eaax8935.
24. Gu, H., Lee, S.W., Carnicelli, J., Zhang, T., and Ren, D. (2020). Magnetically driven active topography for long-term biofilm control. Nat. Commun. *11*, 2211.
25. Hwang, G., Paula, A.J., Hunter, E.E., Liu, Y., Babeer, A., Karabucak, B., Stebe, K., Kumar, V., Steager, E., and Koo, H. (2019). Catalytic antimicrobial robots for biofilm eradication. Sci. Robot. *4*, eaaw2388. https://doi.org/10.1126/scirobotics.aaw2388.
26. Pocivavsek, L., Ye, S.H., O'Dea, R., Tzeng, E., Pugar, J., O'Dea, R., Velankar, S., and Cerda, E. (2018). Topography-driven surface renewal. Nat. Phys. *14*, 948–953. https://doi.org/10.1038/s41567-018-0193-x.
27. Zhao, L., Li, W., Liu, Y., Qi, Y., An, N., Yan, M., Wang, Z., Zhou, M., and Yang, S. (2024). Designing Fast-Moving Antibacterial Microtorpedoes to Treat Lethal Bacterial Biofilm Infections. ACS Nano *18*, 19712–19722. https://doi.org/10.1021/acsnano.4c04995.
28. Wang, J., Wang, L., Sun, N., Tierney, R., Li, H., Corsetti, M., Williams, L., Wong, P.K., and Wong, T.-S. (2019). Viscoelastic solid-repellent coatings for extreme water saving and global sanitation. Nat. Sustain. *2*, 1097–1105. https://doi.org/10.1038/s41893-019-0421-0.
29. Park, A., Jeong, H.H., Lee, J., Kim, K.P., and Lee, C.S. (2011). Effect of shear stress on the formation of bacterial biofilm in a microfluidic channel. BioChip J. *5*, 236–241. https://doi.org/10.1007/s13206-011-5307-9.
30. Nejadnik, M.R., van der Mei, H.C., Busscher, H.J., and Norde, W. (2008). Determination of the shear force at the balance between bacterial attachment and detachment in weak-adherence systems, using a flow displacement chamber. Appl Environ Microb *74*, 916–919. https://doi.org/10.1128/Aem.01557-07.
31. Roosjen, A., Boks, N.P., van der Mei, H.C., Busscher, H.J., and Norde, W. (2005). Influence of shear on microbial adhesion to PEO-brushes and glass by convective-diffusion and sedimentation in a parallel plate flow chamber. Colloid Surface B *46*, 1–6. https://doi.org/10.1016/j.colsurfb.2005.08.009.
32. Busscher, H.J., and van der Mei, H.C. (2006). Microbial adhesion in flow displacement systems. Clin. Microbiol. Rev. *19*, 127–141. https://doi.org/10.1128/Cmr.19.1.127-141.2006.
33. Raya, A., Sodagari, M., Pinzon, N.M., He, X., Zhang Newby, B.M., and Ju, L.K. (2010). Effects of rhamnolipids and shear on initial attachment of PAO1 in glass flow chambers. Environ Sci Pollut R *17*, 1529–1538. https://doi.org/10.1007/s11356-010-0339-6.
34. Boks, N.P., Norde, W., van der Mei, H.C., and Busscher, H.J. (2008). Forces involved in bacterial adhesion to hydrophilic and hydrophobic surfaces. Microbiol-Sgm *154*, 3122–3133. https://doi.org/10.1099/mic.0.2008/018622-0.
35. Wang, H., Sodagari, M., Ju, L.K., and Zhang Newby, B.m. (2013). Effects of shear on initial bacterial attachment in slow flowing systems. Colloid Surface B *109*, 32–39. https://doi.org/10.1016/j.colsurfb.2013.03.016.
36. Reddy, K., and Ross, J.M. (2001). Shear Stress Prevents Fibronectin Binding Protein-Mediated *Staphylococcus aureus* Adhesion to Resting Endothelial Cells. Infect. Immun. *69*, 3472–3475. https://doi.org/10.1128/iai.69.5.3472-3475.2001.
37. Ma, Z., Bumunang, E.W., Stanford, K., Bie, X., Niu, Y.D., and McAllister, T.A. (2019). Biofilm Formation by Shiga Toxin-Producing Escherichia coli on Stainless Steel Coupons as Affected by Temperature and Incubation Time. Microorganisms *7*, 95.
38. Peleg, A.Y., and Hooper, D.C. (2010). Hospital-acquired infections due to gram-negative bacteria. N. Engl. J. Med. *362*, 1804–1813.
39. Qi, S., Wang, J., Cheng, D., Pan, T., Tan, R., Qu, H., and Zhu, L.-M. (2025). Rational Design of Microbicidal Inorganic Nano-Architectures. Small, 2502663. https://doi.org/10.1002/smll.202502663.
40. Amini, S., Kolle, S., Petrone, L., Ahanotu, O., Sunny, S., Sutanto, C.N., Hoon, S., Cohen, L., Weaver, J.C., Aizenberg, J., et al. (2017). Preventing mussel adhesion using lubricant-infused materials. Science *357*, 668–673. https://doi.org/10.1126/science.aai8977.
41. Kuzina, M.A., Kartsev, D.D., Stratonovich, A.V., and Levkin, P.A. (2023). Organogels versus Hydrogels: Advantages, Challenges, and Applications. Adv. Funct. Mater. *33*, 2301421. https://doi.org/10.1002/adfm.202301421.

42. Wang, J., Wu, B., Dhyani, A., Repetto, T., Gayle, A.J., Cho, T.H., Dasgupta, N.P., and Tuteja, A. (2022). Durable Liquid- and Solid-Repellent Elastomeric Coatings Infused with Partially Crosslinked Lubricants. ACS Appl. Mater. Interfaces *14*, 22466–22475. https://doi.org/10.1021/acsami.2c03408.

43. Rauch, K.D., Bennett, J.L., Stoddart, A.K., and Gagnon, G.A. (2024). UV LED disinfection as a novel treatment for common salmonid pathogens. Sci. Rep. *14*, 28392. https://doi.org/10.1038/s41598-024-79347-6.

44. Jiang, S., and Cao, Z. (2010). Ultralow-Fouling, Functionalizable, and Hydrolyzable Zwitterionic Materials and Their Derivatives for Biological Applications. Adv. Mater. *22*, 920–932. https://doi.org/10.1002/adma.200901407.

45. Dai, G., Xie, Q., Ai, X., Ma, C., and Zhang, G. (2019). Self-Generating and Self-Renewing Zwitterionic Polymer Surfaces for Marine Anti-Biofouling. ACS Appl. Mater. Interfaces *11*, 41750–41757. https://doi.org/10.1021/acsami.9b16775.

46. Elbourne, A., Cheeseman, S., Atkin, P., Truong, N.P., Syed, N., Zavabeti, A., Mohiuddin, M., Esrafilzadeh, D., Cozzolino, D., McConville, C.F., et al. (2020). Antibacterial Liquid Metals: Biofilm Treatment via Magnetic Activation. ACS Nano *14*, 802–817. https://doi.org/10.1021/acsnano.9b07861.

47. Widmer, A.F., and Frei, R. (2011). Decontamination, disinfection, and sterilization. In Manual of Clinical Microbiology, pp. 143–173.

48. Suzuki, A., Emoto, A., Shirai, A., and Nagamatsu, K. (2022). Ultraviolet light-emitting diode (UV-LED) sterilization of citrus bacterial canker disease targeted for effective decontamination of Citrus sudachi fruit. Biocontrol Sci. *27*, 1–7.